

Quantum Monte Carlo simulation of light and superlight bipolarons in extended Hubbard–Holstein models on face- and body-centered-cubic lattices

G D Adebajo J P Hague P E Kornilovitch

G D Adebajo and J P Hague

School of Physical Sciences, The Open University, Walton Hall, Milton Keynes, MK7 6AA, UK

Email Address: Jim.Hague@open.ac.uk

P E Kornilovitch

Department of Physics, Oregon State University, Corvallis, OR, 97331, USA

Superlight pairing of bipolarons driven by electron-phonon interactions (EPIs) in face-center-cubic (FCC) and body-center-cubic (BCC) lattices is investigated using a continuous-time path-integral quantum Monte Carlo (QMC) algorithm. The EPIs are of the Holstein and extended Holstein types, and a Hubbard interaction is also included. The number of phonons associated with the bipolaron, inverse mass, and radius are calculated and used to construct a phase diagram for bipolaron pairing (identifying the regions of pairing into intersite bipolarons and onsite bipolarons). From the inverse mass it is determined that for the extended interaction, there is a region of light pairing associated with intersite bipolarons formed in both BCC and FCC lattices. Intersite bipolarons in the extended model at large phonon frequency and large Coulomb repulsion become superlight due to first order hopping effects. The transition temperature of Bose–Einstein condensates of these pairs is estimated. It is determined that intersite bipolarons are associated with regions of high transition temperatures.

Keywords: *Superconductivity, unconventional superconductivity, bipolarons, UV model*

1 Introduction

The discovery of cuprate superconductors stimulated searches for other materials that could superconduct at high temperatures. Among them are the A_3C_{60} materials [1], which are doped from C_{60} insulators [2] (where A is Cs, Rb or K) and are unconventional superconductors with high transition temperatures (up to 38 K [3]), large Coulomb repulsion, and Jahn–Teller coupling (which has similarities to other electron-phonon couplings). The cesium-doped solid (Cs_3C_{60}) can have both BCC (cubic A15) and FCC structures which superconduct at similar temperatures under pressure [3, 4, 5]. The materials have an s -wave order parameter with signatures of unconventional superconductors such as the proximity of Mott and superconducting states [6] and BCS-like theories may be insufficient to explain the superconducting mechanism in these compounds [7, 8, 9]. As such, we are motivated to determine the properties of BCC and FCC bipolarons in systems with strong interactions between phonon modes and electrons in the presence of strong Coulomb repulsion.

We will consider the extended Hubbard–Holstein model (EHHM), which has the following form:

$$H = -t \sum_{\langle ii' \rangle \sigma} c_{i\sigma}^\dagger c_{i'\sigma} + \hbar\omega \sum_{ij\sigma} g_{ij} n_{i\sigma} \left(a_j^\dagger + a_j \right) + \hbar\omega \sum_j \left(a_j^\dagger a_j + \frac{1}{2} \right) + U \sum_i n_{i\downarrow} n_{i\uparrow}, \quad (1)$$

where g_{ij} is a dimensionless electron phonon interaction strength, c_i (c_i^\dagger) annihilate (create) electrons and the a_j (a_j^\dagger) operators do the same for phonons on site j . t is the hopping between neighboring sites. U is the on site Coulomb repulsion (Hubbard U). The phonon frequency is ω . The Holstein model corresponds to $g_{ij} = g\delta_{ij}$. The extended Holstein interaction considered here (following Ref. [10]) only shares phonons between sites on nearest-neighbour bonds.

In the limit of large phonon frequency, a Lang–Firsov approximation leads to decoupling of phonons and electrons since the average number of phonons in the wavefunction is zero in that limit (where it takes a large quantity of energy to create a phonon), to obtain,

$$\tilde{H}_{\text{LF}} = -t \sum_{\langle ii' \rangle} \exp \left[-\frac{W\lambda\gamma}{\hbar\omega} \right] c_i^\dagger c_{i'} + \sum_{ii'} n_i n_{i'} \left(\frac{U}{2} \delta_{ii'} - \frac{W\lambda\Phi_{ii'}}{\Phi_{00}} \right) - \sum_i U n_i + \hbar\omega \sum_j \left(a_j^\dagger a_j + \frac{1}{2} \right) \quad (2)$$

where the effective phonon-mediated interaction has the form,

$$\Phi_{ii'} = \hbar\omega \sum_j g_{ij}g_{ji'}, \quad (3)$$

and we used Φ_{NN} to denote near-neighbour phonon-mediated coupling. Here, the non-interacting half bandwidth, $W = zt$, where z is the number of near neighbours and we defined $\gamma = 1 - \Psi_{\text{NN}}/\Phi_{00}$. For the Holstein and extended Holstein interactions considered, $\Phi_{ii'}$ is only non-zero for on-site and near-neighbor sites. The electron-phonon interaction strength is,

$$\lambda = \frac{\Phi_{00}}{W}. \quad (4)$$

Thus the effective on-site and inter-site coupling strengths are $U' = U - 2W\lambda$ and $V' = -2W\lambda\Phi_{\text{NN}}/\Phi_{00}$. Bipolarons formed in the Holstein-Hubbard model (HHM) and those formed in a truncated EHHM [10] consist of two polarons that can bind into a stable pair when the exchange of phonons overcomes Coulomb repulsion. These categories of bipolarons differ in the spatial extent of their EPI. As shown schematically in Figure 2, the nature of the EPI in the HHM is site-local (electron located at the vibrating atomic site) whereas the EHHM has a long-range EPI (of near-neighbour type). To our knowledge, there are no numerical studies yet of bipolaron properties in either the BCC or the FCC lattice. We note our previous QMC studies of bipolarons on the chain [11], square lattice [12], triangular lattice [13, 12] and simple cubic lattice [14].

The transition temperature of a superconductor of real-space bipolarons in the BEC regime depends critically on their mass and size. In the dilute limit, where there is infrequent scattering *between* bipolarons, the transition temperature has the form,

$$T_{\text{BEC}} = \frac{3.31\hbar^2 n_b^{2/3}}{k_B m^{**}}, \quad (5)$$

where m^{**} is the bipolaron (pair) mass, and n_b is their density. As n_b increases, T_{BEC} also increases until bipolarons start to overlap, at which point the transition temperature saturates before decreasing. Saturation of T_{BEC} is estimated to occur in the vicinity of *close packing*. Thus, a close packing transition temperature is defined to be [15]

$$\frac{k_B T^*}{t} \sim \frac{6.62 m_0}{\Omega_p^{2/3} m^{**}}, \quad (6)$$

where the bare *electron* mass is $m_0 = \hbar^2/(2ta^2)$, and Ω_p is the bipolaron volume in units of the lattice constant a . Ω_p needs to be small enough such that inter-bipolaron scattering does not significantly affect Eq. (5).

As can be appreciated from Eqs. (5) and (6), the critical temperature is inversely proportional to the bipolaron mass. Thus in the context of superconductivity, it is important to understand when bipolarons are heavy and when they may be light. The range of electron-phonon interaction affects m^{**} in two crucial ways.

First, it affects the *polaron* mass (i.e. the mass of the two bipolaron constituents), $m^* \sim m_0 \exp(\gamma W\lambda/\hbar\omega)$ (in the limit of large $\hbar\omega/W$). For the local interaction of the HHM, the lattice deformation is confined to the site occupied by the fermion and is very localised. When the polaron moves, the entire deformation must move to the neighboring site resulting in an exponentially large m^* , since $\gamma = 1$ for the HHM. In the EHHM, the lattice on the nearest site is partially pre-deformed. *Additional* deformation associated with polaron movement is smaller than in the Holstein case, which leads to $\gamma < 1$. Thus, EHHM polarons can be *exponentially* lighter than HHM polarons. We call such polarons “light” [16].

The second effect of the interaction range is related to bipolaron movement. In the HHM, both polarons occupy the same lattice site in the S0 (on-site singlet) configuration. Bipolaron movement is a second-order process that involves an intermediate state with energy excess equal to the bipolaron binding energy Δ . As a result, the bipolaron mass scales as $m^{**} \propto (m^*)^2 \Delta$ in the antiadiabatic limit. Holstein

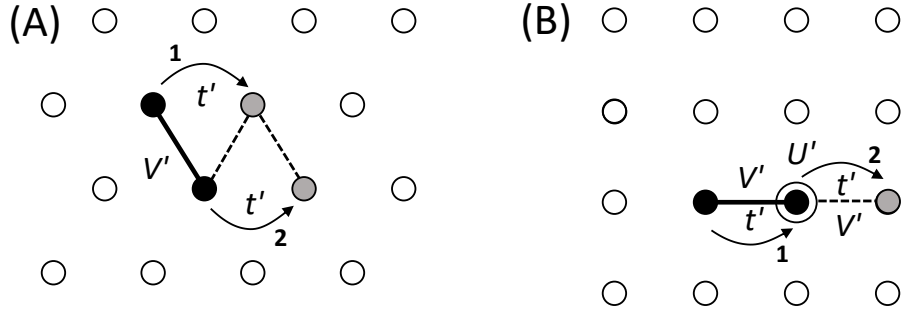


Figure 1: Schematics of different light pair mechanisms. (A) On the triangular lattice, a pair with NN attraction V' moves in the first order of NN hopping t . (B) In the resonant case, $V' = U'$, the pair can move in the first order of NN hopping t even on the square lattice. Numbers ‘1’ and ‘2’ indicate hopping order.

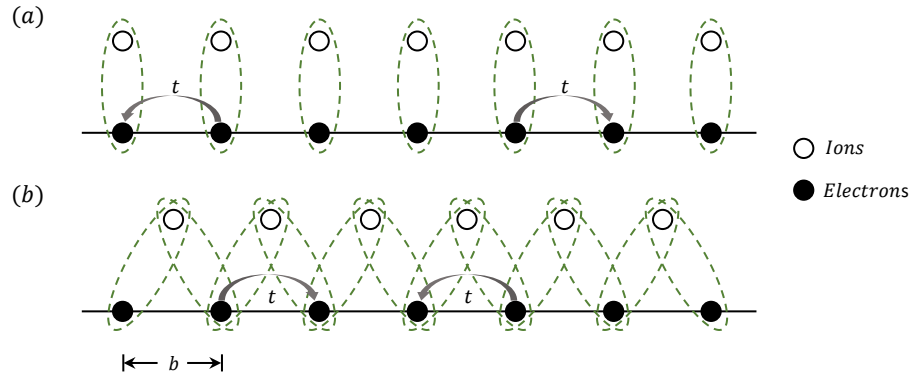


Figure 2: One-dimensional schematic of (a) the Holstein-Hubbard model and (b) the extended Holstein-Hubbard model with near-neighbour EPI introduced in Ref. [10] and studied here. The filled circles, empty circles and dashed oval circles represent the electron Wannier orbitals, lattice ions, and nonzero electron-phonon coupling, respectively. The nearest-neighbour electron sites have overlapping orbitals such that an electron can hop via t , and b is the intersite spacing.

bipolarons are exponentially heavier than Holstein polarons. This result applies to Holstein models in lattices of all dimensionalities. The same scaling $m^{**} \propto (m^*)^2 \Delta$ applies to extended EHHM bipolarons on the BCC lattice, although in this case the constituent polarons are light and therefore the bipolaron is also light. However, EHHM bipolarons on the FCC lattice may display a qualitatively different behavior. If the Hubbard repulsion is strong enough, the two polarons will be forced to occupy two neighbouring sites in S1 configuration. Due to the geometry of the FCC lattice, the S1 bipolaron can move in the *first order* in polaron hopping in the large ω limit, as illustrated in Figure 1. The S1 bipolaron mass scales as $m^{**} \propto m^*$. We call such bipolarons “superlight” [16].

We expect, therefore, all HHM bipolarons to be very heavy and suppress T^* . The EHHM bipolarons on the BCC lattice are expected to be light with an intermediate T^* . On the FCC lattice, the EHHM bipolarons are light in the S0 configuration and superlight in the S1 (intersite singlet) configuration. The latter provides the highest T^* .

The goal of this study is to understand whether the above qualitative picture is maintained as ω is lowered towards the adiabatic limit using a numerically exact QMC simulation method. The paper is organised as follows: In Section 2 an overview of the quantum Monte Carlo scheme is given, in addition to introducing a new triple update needed when simulating FCC lattices in section 2.1 (further details of this scheme can be found in the Appendix). In Section 3 results from the simulations are presented. Finally, in Section 4 a summary can be found.

2 Method

In this work, we use a continuous-time path-integral quantum Monte Carlo scheme to simulate the HHM and EHHM (see e.g. Refs. [16, 12, 14]). We place two fermions in a $20 \times 20 \times 20$ box (BCC and FCC lattices, respectively), and then carry out simulations for $\bar{\beta} = t/k_B T = 20$ (where k_B is Boltzmann's constant and T the temperature) at phonon frequencies of $\hbar\omega/t = 1$ and $\hbar\omega/W = 1$. A range of U and λ are simulated. We adopt twisted boundary conditions on path ends to estimate the mass. Detailed procedures for the simulation and evaluation of estimators for a range of bipolaron properties have been discussed in earlier papers (see Refs. [11, 12, 14], and references therein). Measurements are made every few Monte Carlo steps.

We use the update scheme summarised in Appendix A for BCC lattices (which is essentially the same set of updates as for simple cubic lattices). For FCC lattices, these updates plus an additional update analogous to the triple update are needed to simulate bipolarons on triangular lattices (see Ref. [16]) is also required.

2.1 Three-kink update for FCC Lattice

Due to the geometry of the FCC lattice, it is possible that a bound bipolaron returns to its initial configuration after three consecutive nearest-neighbour hops of one of the particles. Hence, an update with this property needs to be in the Monte Carlo scheme when simulating FCC lattices to ensure ergodicity. The update procedure is as follows:

1. One of two paths is selected with equal probability $1/2$.
2. A combination of three kinks that is suitable for this update is determined. A kink is selected from the 12 possible kinks (the number of nearest-neighbour sites) and we label it \mathbf{l}_1 . Then, we choose two other kinks at random (\mathbf{l}_2 and \mathbf{l}_3) such that $\mathbf{l}_1 + \mathbf{l}_2 + \mathbf{l}_3 = 0$. Satisfying this condition means that the particle returns to its initial site after three hops. None of these three kinks is an antikink to any other.
3. We choose insertion or removal of the (three) kinks with equal probability $1/2$.
4. If insertion is chosen during Step 4, we select the imaginary times τ_1, τ_2, τ_3 for the new kinks with equal probability $1/\bar{\beta}$ from the interval $[0, \bar{\beta})$. The Metropolis condition is given as:

$$P_{\text{add}}(\tau_1, \tau_2, \tau_3) = \min \left\{ 1, \frac{\bar{\beta}}{N_{\mathbf{l}_1} + 1} \frac{\bar{\beta}}{N_{\mathbf{l}_2} + 1} \frac{\bar{\beta}}{N_{\mathbf{l}_3} + 1} \cdot e^{A(D) - A(C)} \right\} \quad (7)$$

where C and D are the initial and final configurations, respectively. $A(C)$ and $A(D)$ are the bipolaron actions in both initial and final configurations (see Refs. [11, 12, 14]). $N_{\mathbf{l}_i}$ ($i = 1, 2, 3$) is the number of kinks of type \mathbf{l}_i before the addition update (i.e. in the initial configuration, C).

5. On the other hand, if removal of kinks is selected in Step 4, there are two possibilities. The first is to check whether the kink types $\mathbf{l}_1, \mathbf{l}_2$, and \mathbf{l}_3 chosen from Step 3 already exist in the initial configuration. If any of those selected kinks does not exist in the current path, the acceptance probability is zero and the update is aborted. Otherwise, provided that there is at least one kink of each type, the removal at imaginary times associated with the selected kinks, τ_1, τ_2, τ_3 , is carried out with the acceptance probability:

$$P_{\text{remove}}(\tau_1, \tau_2, \tau_3) = \min \left\{ 1, \frac{N_{\mathbf{l}_1}}{\bar{\beta}} \frac{N_{\mathbf{l}_2}}{\bar{\beta}} \frac{N_{\mathbf{l}_3}}{\bar{\beta}} \cdot e^{A(C) - A(D)} \right\} \quad (8)$$

where $N_{\mathbf{l}_i}$ ($i = 1, 2, 3$) is the number of kinks of type \mathbf{l}_i before removal.

We note that other 3 kink updates are possible, but the selected update is sufficient to ensure ergodicity.

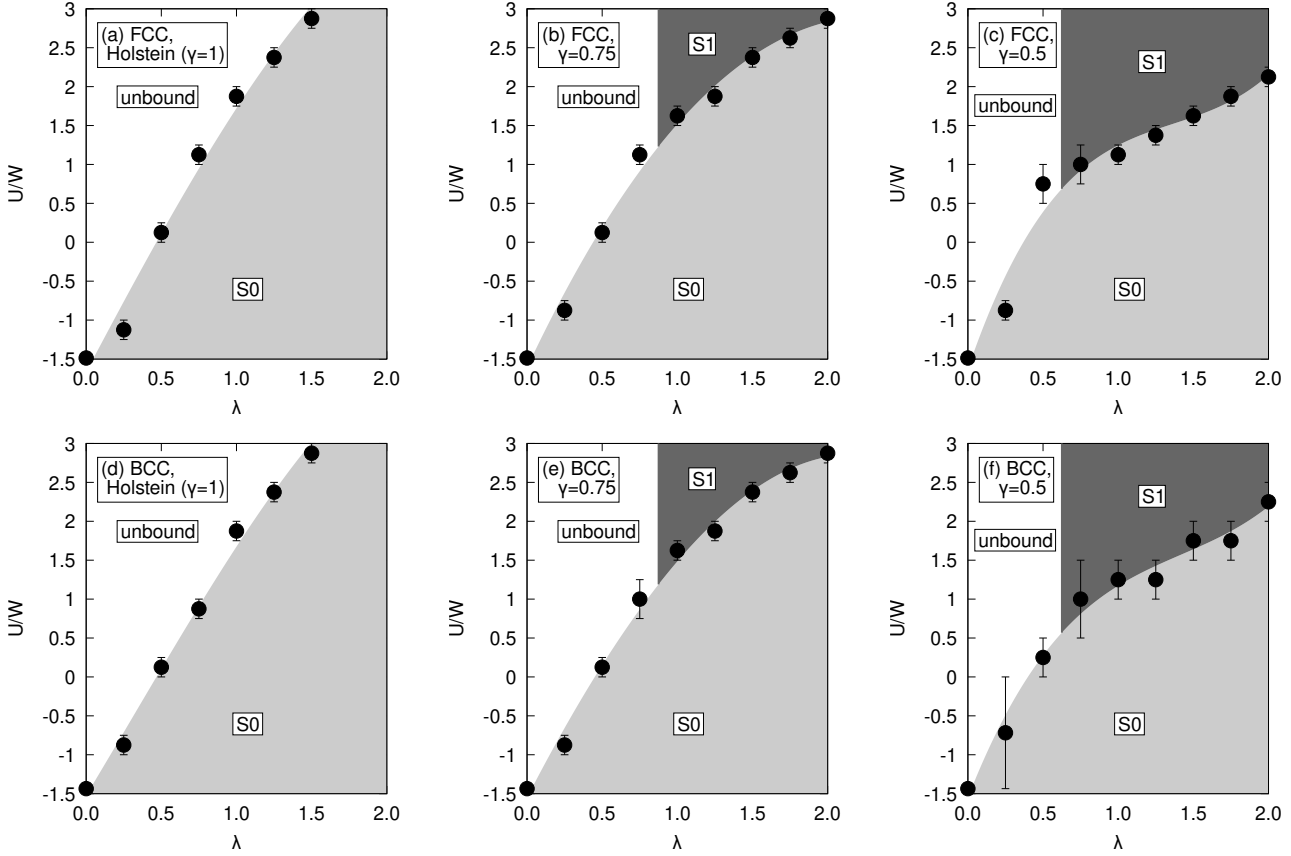


Figure 3: Phase diagram of the extended Holstein model on BCC and FCC lattices shown for three different values of $\gamma = 1 - \Phi_{NN}/\Phi_{00}$. The additional intersite interaction promotes S1 pairing leading to an increase in the size of the S1 region such that it can be found at lower U and λ . The case $\gamma = 1$ corresponds to the Holstein interaction. Lines are a guide to the eye, determined by fitting a cubic curve to the points defining the S0 boundary.

3 Results

This section describes singlet bipolarons in both the HHM and EHHM. Properties of the bipolarons are computed for both BCC and FCC lattices, and include the ground state energy, the total number of excited phonons, the effective mass, and the bipolaron radius. From these, the phase diagram is determined. The phase (binding) diagram of the Holstein and extended Holstein bipolarons is shown in Fig. 3. The S0 part of the phase diagram was determined by searching for a sudden drop in the number of phonons associated with the two particles as U is increased at fixed λ followed by a region where there is no change in N_{ph} on further increase in U . For the regions of parameter space with no S0 bipolaron, the S1 bipolaron is identified by determining where the particle separation is the intersite spacing, b and unbound cases where the particle separation is very large. For FCC lattice, $b = a/\sqrt{2}$ and for BCC lattice, $b = a\sqrt{3}/2$. The Holstein cases are shown in panels (a) and (d). We have not identified an S1 region in this case, although we note that a tiny S1 region can be observed for the 2D Holstein bipolaron [17].

An abrupt change in the number of phonons, N_{ph} , associated with the bipolaron can be found at the boundary of the region of parameter space containing S0 states (Fig. 4). For unbound states and S1 states, N_{ph} and other properties do not vary on change of the site local Hubbard U . For the unbound case, the abrupt change occurs because there is a smaller phonon cloud associated with a polaron than a bipolaron (the bipolaron self reinforces the phonon cloud). There are also fewer phonons associated with the S1 bipolaron, since the electron-phonon interaction is stronger on-site than intersite, so there is less opportunity to create phonons.

Figure 5 shows the inverse radius of the bipolaron. Again computations are shown for BCC and FCC lattices and a range of γ is considered. The regions of the parameter space where S1 bipolaron are formed can be determined by finding pairs with interparticle spacing, b . This region can be identified as an area

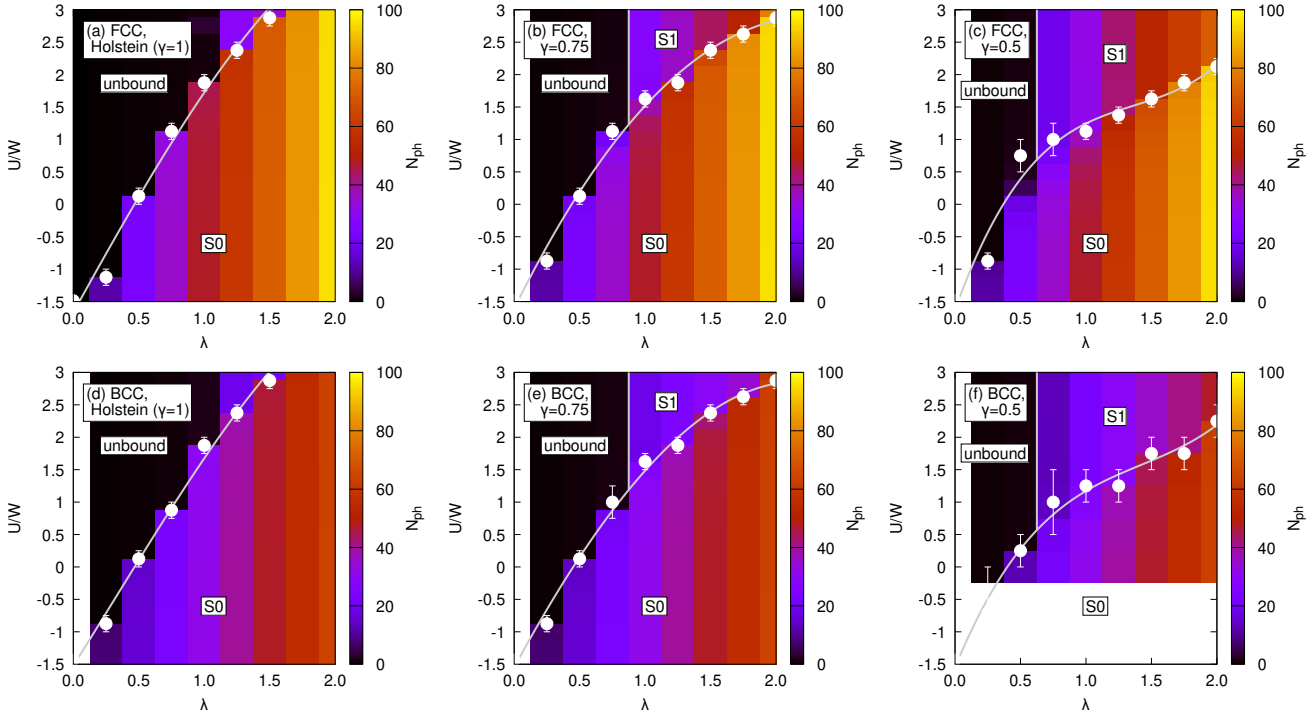


Figure 4: Number of phonons associated with the bipolaron. An abrupt change in the number of phonons corresponds to the boundary between S0 and S1 bipolarons. There are approximately 50% more phonons associated with the FCC lattice due to the larger kinetic energy relative to $\hbar\omega$ in that case. N_{ph} is constant on change of U for S1 and unbound cases.

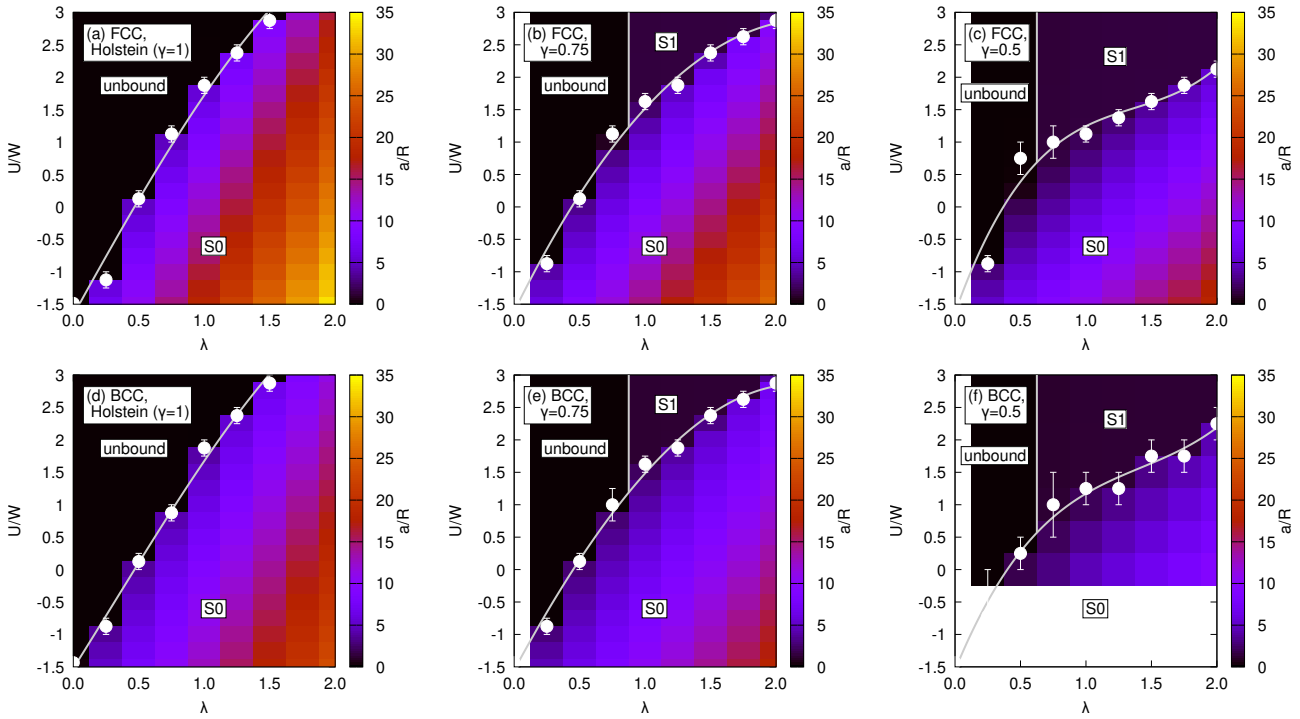


Figure 5: Inverse radius of the bipolaron, a/R . The S1 bipolaron is characterized by pairs with interparticle spacing, b at large U and large λ . The S0 bipolaron is small and characterized by large inverse radius (found for large λ and small U). Regions with no pairing are found for large U and small λ and shown in black.

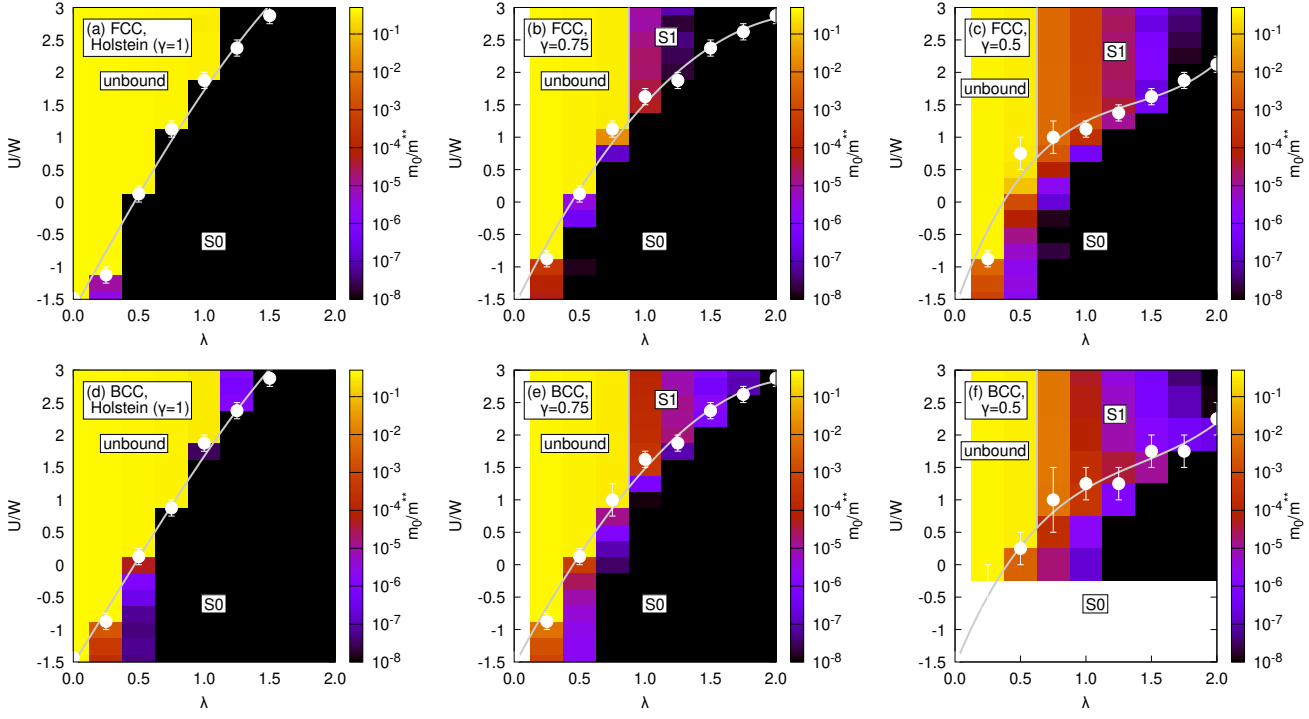


Figure 6: Inverse mass of the bipolaron in units of the electron mass, m_0/m^{**} . $\hbar\omega = t$ in both cases. A sharp change is found at the boundary of the S0 region of the binding diagram.

of constant a/R in the upper right corner of the plots for large U and large λ . The S0 bipolaron is smaller than the intersite spacing showing as a large inverse radius (found for large λ and small U such that the electron-phonon coupling overcomes the Coulomb repulsion). Regions with no pairing are found for large U and small λ such that Coulomb repulsion overcomes the electron-phonon coupling and are shown in black. We note that inverse radius is displayed so that the unbound regions (with large radius) do not dominate the plot.

We show the inverse mass of the bipolarons in Fig. 6. The S0 bipolaron is typically much heavier than the S1 bipolaron, and is typically only light close to the edge of the S0 region. For the $\hbar\omega = t$ cases, the S1 bipolaron is lighter for the $\gamma = 0.5$ case and heavier for the $\gamma = 0.75$ case. Generally the Holstein bipolaron is heaviest. We note that for the FCC cases, $\hbar\omega = t$ is further into the adiabatic regime, since $\hbar\omega/W$ is smaller due to the larger band width.

Figure 7 shows transition temperature estimates. The FCC bipolaron has a higher maximum transition temperature than the BCC case for $\gamma = 0.5$, in spite of the larger polaron mass. For $\gamma = 0.75$, the BCC case has the higher transition temperature. There is a small region of large S0 bipolaron with higher estimated transition temperature in the Holstein case at small U and λ . Since the pairs are large for the S0 bipolaron the system approaches the BCS rather than BEC limit in for $\lambda \rightarrow 0$. We note again that the ratio $\hbar\omega/W$ is smaller in the FCC than the BCC case so that there is more phonon creation and this may lead to a lowering of the relative transition temperature. In spite of this, the transition temperature is slightly higher for the FCC case with $\gamma = 0.5$ over parts of the parameter space containing the S1 bipolaron.

Figure 8 shows the inverse mass, number of phonons, inverse radius and estimated transition temperature of the FCC and BCC bipolarons at large λ and $\hbar\omega = W$. The FCC bipolaron is lighter than the BCC case by around 50% in this limit, with the S1 bipolaron much lighter than the S0 bipolaron in all cases. At the larger λ , the bipolaron is slightly lighter at the boundary between the S0 and S1 bipolarons, as a manifestation of the crawler resonance of the bipolaron which can be identified in the antiadiabatic limit (where the on-site and intersite bipolaron configurations have similar energy) as in Fig. 1(B). The superlight mechanisms that we have previously discussed have been established for the anti-adiabatic limit of high phonon frequency. We therefore expect systems with large phonon frequencies (typically

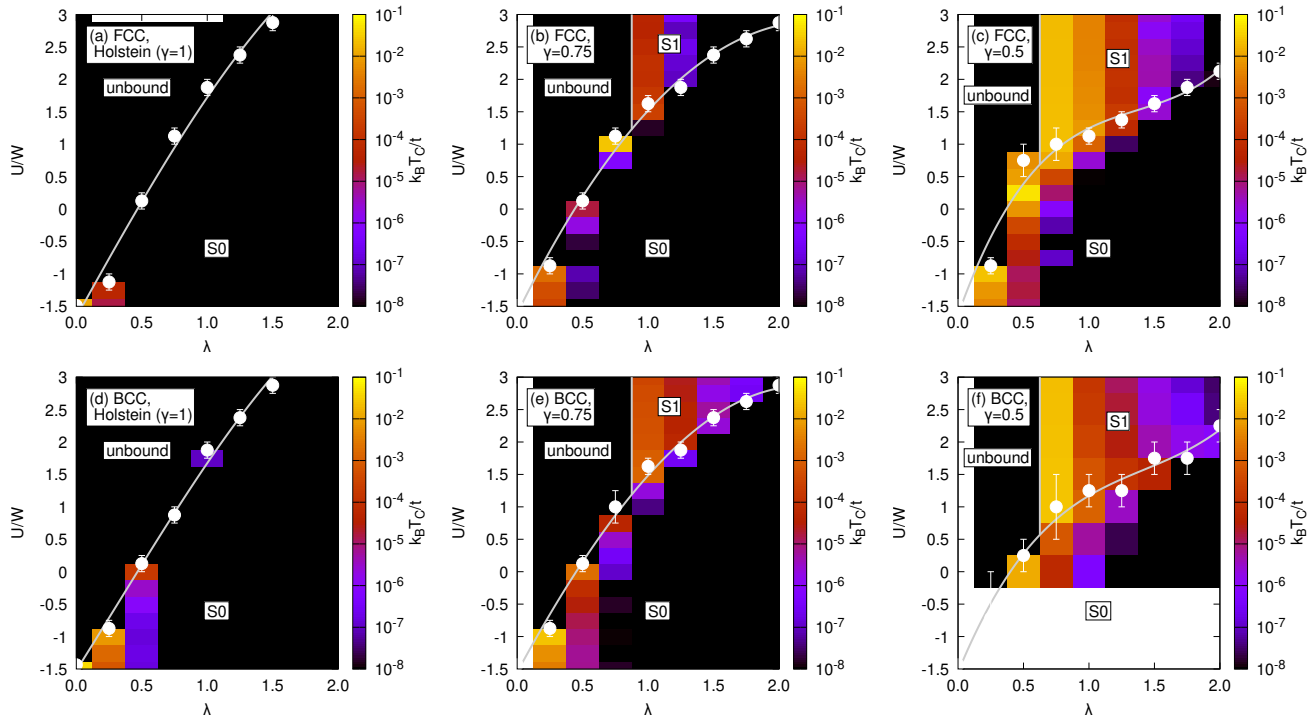


Figure 7: Transition temperature estimates. The FCC bipolaron has a higher maximum transition temperature than the BCC case for $\gamma = 0.5$, in spite of the larger polaron mass. For $\gamma = 0.75$, the BCC case has a higher transition temperature. There is a small region of higher T_C associated with large bipolarons at low U and λ for $\gamma = 1$ (Holstein model) that is outside the BEC regime.

the case in systems with low kinetic energies) to have more signatures of this superlight mechanism. At phonon frequency $\hbar\omega = W$, the number of phonons associated with the bipolaron shows a smoother crossover between the S0 and S1 states. The number of phonons is much smaller than for the $\hbar\omega = t$ case reflecting the additional energy carried with the phonons in the bipolaron cloud. The inverse radius displays similar behaviour to the $\hbar\omega = t$ case.

Finally, the estimated transition temperature is shown in Panel 8(d). The estimated transition temperature is much higher in the FCC case than the BCC case, and the ratio of the transition temperatures for the two cases increases with the electron-phonon coupling strength as the bipolaron becomes more tightly bound between sites and the superlight effect becomes more important. The bipolarons become lighter at the point where the on-site and intersite effective interactions become similar. We do not notice a peak in the estimated transition temperature associated with $U' \sim V'$ in either the BCC or FCC cases.

4 Discussion and conclusions

Using continuous time path-integral QMC simulations, we have studied the bipolaron in the Hubbard–Holstein and extended Hubbard–Holstein models, which contain local Coulomb repulsion in the presence of phonon-mediated attractive interactions. We have focussed on pairing in BCC and FCC lattices. We used N_{ph} and R to determine the binding (phase) diagram. Mass was calculated using twisted boundary conditions. Transition temperatures were estimated. A benefit of the QMC simulation is that we can examine the effect of phonon retardation on the properties of bipolarons. When $\hbar\omega \ll W$, the retardation effects are significant.

We found that intersite interactions lead to qualitatively different pair properties: strongly bound EHHM bipolarons form both S0 and S1 pairs whereas HHM bipolarons are only found to have onsite characteristics. Specifically, at large U and $\lambda \gtrsim 1$, HHM and EHHM bipolarons have qualitatively different behaviours: intersite EHHM bipolarons can be well bound and stable at large U above a critical electron-

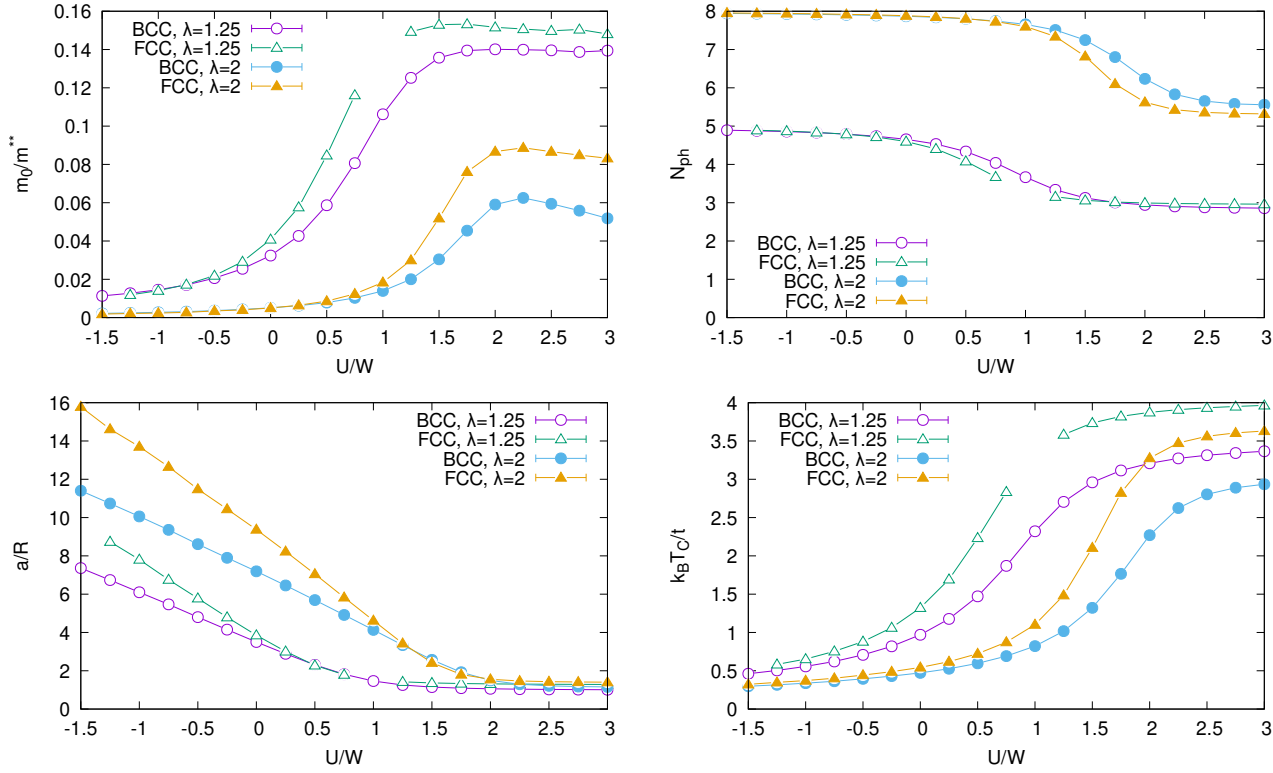


Figure 8: Inverse mass, N_{ph} , inverse radius and estimated transition temperature of the FCC and BCC bipolarons at large λ and $\hbar\omega = W$. The FCC bipolaron is lighter (superlight) in this limit, with the S1 bipolaron much lighter than the S0 bipolaron in all cases. The small peak in inverse mass for $\lambda = 2$ and BCC lattice (and to a lesser extent for the FCC lattice) corresponds to the light bipolaron case where intra and inter-site effective interactions are of similar size on the boundary between S0 and S1 bipolarons. For larger phonon frequency, the number of phonons changes more slowly at the boundary between S0 and S1 bipolarons. Transition temperature increases monotonically with U . $\gamma = 0.5$. As λ increases, the percentage difference between the BCC and FCC cases becomes larger as the superlight regime is approached. For each data point, the error bars are displayed as 3 standard deviations. Where the error bars are not visible it means that they are too small to be apparent on the scale of the plot.

phonon coupling, $\lambda \geq \lambda_C$, due to the near-neighbour phonon attraction. The value of λ_C decreases with decreased γ .

Overall, we found no qualitative difference in bipolaron binding diagrams for BCC and FCC lattices for $\hbar\omega = t$. S1 bipolarons at intermediate electron-phonon coupling tend to be lighter on the FCC lattice for larger intersite coupling and heavier for lower intersite coupling. In the Holstein case, the FCC bipolaron is much heavier and as γ decreases, the FCC is lighter.

On increase of phonon frequency, retardation effects become less important and the effective interaction Hamiltonian becomes more Hubbard like. We observed that for $\hbar\omega = W$, signatures of superlight states (where the pair moves by first-order hops) start to emerge, and lower masses are found for FCC lattices, especially at large λ . We also see evidence of superlight behaviour for pairs on BCC lattices of the type shown in Fig. 1(B) for the specific case where $U' = V'$. Estimated transition temperatures in this case are larger for bipolarons on FCC lattices.

As further work, we think study of the EPIs in A_3C_{60} compounds would be interesting to establish whether any longer range EPIs that could lead to superlight effects are present. Additional QMC calculations including next-nearest neighbour hopping would also be of interest for study of the BCC lattice, since the intersite spacings of near-neighbour and next-nearest neighbour are similar, potentially leading to similar hoppings with other large effects [15]. This is beyond the scope of the current paper as it would require significant algorithmic development with additional 3 kink updates including next-nearest neighbour hopping and is reserved for a future publication.

References

- [1] W. Krätschmer, L. D Lamb, K. Fostiropoulos, and D. R Huffman. Solid C_{60} : a new form of carbon. *Nature*, 347(6291):354–358, 1990.
- [2] L. Forró and L. Mihály. Electronic properties of doped fullerenes. *Rep. Prog. Phys.*, 64(5):649–699, 2001.
- [3] A. Y. Ganin, Y. Takabayashi, Y. Z. Khimyak, S. Margadonna, A. Tamai, M. J. Rosseinsky, and K. Prassides. Bulk superconductivity at 38 K in a molecular system. *Nature Materials*, 7(5):367–371, 2008.
- [4] A. Y. Ganin, Y. Takabayashi, P. Jeglič, D. Arčon, A. Potočnik, P. J. Baker, Y. Ohishi, M. T McDonald, M. D. Tzirakis, A. McLennan, et al. Polymorphism control of superconductivity and magnetism in Cs_3C_{60} close to the Mott transition. *Nature*, 466(7303):221–225, 2010.
- [5] Y. Ihara, H. Alloul, P. Wzietek, D. Pontiroli, M. Mazzani, and M. Riccò. NMR study of the Mott transitions to superconductivity in the two Cs_3C_{60} phases. *Phys. Rev. Lett.*, 104:256402, 2010.
- [6] H. Alloul, Y. Ihara, T. Mito, P. Wzietek, M. Aramini, D. Pontiroli, and M. Ricco. NMR investigation of the pressure induced Mott transition to superconductivity in Cs_3C_{60} isomeric compounds. *J. Phys.: Conf. Series*, 449:012030, 2013.
- [7] Y. Nomura, S. Sakai, M. Capone, and R. Arita. Exotic s-wave superconductivity in alkali-doped fullerides. *J. Phys.: Condens. Matter*, 28(15):153001, 2016.
- [8] M. Capone, M. Fabrizio, C. Castellani, and E. Tosatti. Colloquium: Modeling the unconventional superconducting properties of expanded A_3C_{60} fullerides. *Rev. Mod. Phys.*, 81:943–958, 2009.
- [9] O. Gunnarsson. Superconductivity in fullerides. *Rev. Mod. Phys.*, 69:575–606, Apr 1997.
- [10] J. Bonča and S. A. Trugman. Bipolarons in the extended Holstein Hubbard model. *Phys. Rev. B*, 64:094507, 2001.
- [11] J. P. Hague and P. E. Kornilovitch. Bipolarons from long-range interactions: Singlet and triplet pairs in the screened Hubbard-Fröhlich model on the chain. *Phys. Rev. B*, 80:054301, 2009.

- [12] J. P. Hauge and P. E. Kornilovitch. Light and stable triplet bipolarons on square and triangular lattices. *Phys. Rev. B*, 82:094301, 2010.
- [13] J. P. Hauge, P. E. Kornilovitch, J. H. Samson, and A. S. Alexandrov. Superlight small bipolarons in the presence of a strong Coulomb repulsion. *Phys. Rev. Lett.*, 98:037002, 2007.
- [14] A. R. Davenport, J. P. Hauge, and P. E. Kornilovitch. Mobile small bipolarons on a three-dimensional cubic lattice. *Phys. Rev. B*, 86:035106, 2012.
- [15] G.D. Adebajo, J.P. Hauge, and P.E. Kornilovitch. Ubiquitous light real-space pairing from long-range hopping and interactions. *Physics Letters A*, 507:129474, 2024.
- [16] J. P. Hauge, P. E. Kornilovitch, J. H. Samson, and A. S. Alexandrov. Superlight small bipolarons. *J. Phys.: Cond. Matt.*, 19(25):255214, 2007.
- [17] A. Macridin, G. A. Sawatzky, and M. Jarrell. Two-dimensional Hubbard-Holstein bipolaron. *Phys. Rev. B*, 69:245111, 2004.

A Quantum Monte Carlo: Update Rules and Weighting Scheme

The electron paths are continuous in time and an electron hops between sites via kinks in its path. In an exchange configuration, our result is free from sign problem since we only studied singlet states. The selection of path, insertion or removal of kink, and choosing the kink type is implemented probabilistically. The kink type specifies the direction of particle's hop.

Kink insertion or removal is carried out in pairs so that the end configurations of the paths maintain their boundary conditions. We refer to kink insertions and/or removals as updates and there are rules for carrying out these updates for the simulation of two particles. Four binary updates were used:

1. Kinks of type l are added to or removed from each path.
2. Add or remove a kink of type l and its anti-kink $-l$ to or from one of the paths.
3. Insert a kink of type l to one path and remove another kink of the same type l from the same path. This update only works if there is at least one kink of type l on that path since there will no kink to remove if it is non-existent.
4. Insert a kink of type l from one path and remove an anti-kink $-l$ from the other path.

All the updates above were the existing rules prior to the commencement of this study. The detailed balance equations, electron-phonon action, and Metropolis-Rosenbluth conditions for these updates can be found in Ref. [16]. A new update rule for FCC lattices is detailed in the main text.

The summary of the probabilities for kink selection is given below.

- For N_k number of nearest-neighbours, we choose a kink type l with the probability $P_l = 1/N_k$ and its anti-kink l is determined.
- Since there are only two particles, we select one of the two paths as path A with a probability $1/2$ and label the other as path B .
- We choose a kink shift type with an equal probability $P_{\text{Shift}} = 1/2$. The kink shift can either be top shift (in the direction of l) or bottom shift (in the direction of $-l$).
- To remove the first kink of type l from a path A at imaginary time τ , do so with the probability $1/N_{Al}(I)$, where I is the initial configuration before removal.
- To remove the second kink of type l from path A , this is done with a probability $1/N_{Al}(I)$, where I represents the configuration before removal.

-
- The first kink of type l is inserted at time τ with probability density $p(\tau) = 1/\beta$.
 - For the addition of the second kink of type l at time τ' , do so with a probability density $p(\tau) = 1/\beta$.
 - The shift type of the second kink is dependent on whether it is correlated or anti-correlated with the shift type of the first kink. The inter-path distance is unchanged for correlated insertion but changes for anti-correlated insertion.